Damage Assessment for a Sandwich-Like Panel Using Experimental and Numerical Analysis of Guided Waves

Kaleeswaran Balasubramaniam, Piotr Fiborek, Shirsendu Sikdar, and Pawel H. Malinowski

1 Introduction

Aluminum Nomex sandwich core structure (SCS) materials are mainly used in the automobile and aerospace industry for its high strength to weight ratio. Evaluation of these materials is necessary from time to time to prevent disasters to the entire structures. Barely visible impact damage (BVID) is a type of damage that occurs due to some impact drops or mishandling of tools leading to a small or big indentation in the materials. BVIDs on aluminum or steel creates lesser damage to the structure, but on fiber-reinforced polymers like in glass fiber-reinforced polymer (GFRP) or honeycomb structures cause changes to core/core crush or failure of the matrix, etc. Laser Doppler Vibrometer (LDV) is an advanced non destructive testing (NDT) tool used in the industry to detect damage in the early stage. LDV is reliable, handles large materials, and detects the damage sensitive regions.

The lamb waves or guided waves help to evaluate such defects as they can propagate to long distances and its excitation be achieved by a piezo zirconium titanate (PZT) actuator. These lamb waves get reflected from discontinuities and thus help in clear visualization of the damaged region. The usage of lamb waves in the FRP is well known and mentioned in many papers [1], and similarly usage of LDV methods

K. Balasubramaniam (✉) · P. Fiborek · S. Sikdar · P. H. Malinowski
Institute of Fluid Flow Machinery, Department of Mechanics of Intelligent Structures, Polish Academy of Sciences, Fiszera 14 Street, 80-231, Gdansk, Poland
e-mail: kaleeswaranb@imp.gda.pl

P. Fiborek
e-mail: pfiborek@imp.gda.pl

S. Sikdar
e-mail: ssikdar@imp.gda.pl

P. H. Malinowski
e-mail: pmalinowski@imp.gda.pl

C. K. Mukhopadhyay and R. Mulaveesala (eds.), *Advances in Non-destructive Evaluation*, Lecture Notes in Mechanical Engineering,
https://doi.org/10.1007/978-981-16-0186-6_8

in carbon fiber reinforced polymer (CFRP), aluminum is studied in [2]. When lamb waves interact with the damage region, it gets reflected, mode change occurs, and interference in the wave field occurs. The lamb waves occur in the form of asymmetric and symmetric waves. Thus, with the help of LDV and signal processing methods, the analysis of scattered waves is done. LDV works on the principle of Doppler effect and observation of the Doppler shift in frequency. LDV uses either Nd:YAG laser or helium–neon (He–Ne) laser. LDV finds its application mainly in detecting BVID [3], delamination [4], and debonding analysis [5]. The author [6] talks about honeycomb structures and BVID's. The impact test on GFRP [7] is studied and the use of LDV [8] on a composite plate to analyze wave patterns. The spectral element method (SEM), which was developed for the numerical solution of the laminar fluid flow by Patera [9], combines the flexibility of finite element method (FEM) and fast convergence of spectral methods in the frequency domain. This SEM technique was successfully implemented in the field of modeling the phenomena of elastic wave propagation [10–13].

In this research paper, we have used LDV in analyzing the BVID in a semi-sandwich panel with Nomex core and aluminum skin. The damage caused by impacts at 4 and 10 J is studied. In one region, a small portion of Nomex core is completely removed manually, BVID is studied, and in another region, an indentation with a Nomex core protrusion is studied. The results obtained from LDV are compared with the numerical studies to visualize the damage region. The numerical approach is performed using the spectral element method (SEM) code. The gathered data is processed with the elliptical signal processing method for damage localization with various sensor network arrangements.

2 Experimental and Numerical Process

The investigated object is a structure ($50 \times 50 \times 0.1$ cm^3) with aluminum skin and a Nomex honeycomb core at the back. The BVID is made by a low-impact equivalent to 4 and 10 J from the Nomex core side. On one side, a small portion of Nomex cells are manually removed to create a BVID, and another BVID is made with the crushing of Nomex cells. The device used to create the BVID is a circular impactor of 10 cm diameter. The specimen is shown in Fig. 1a. The largest diameter BVID is zoomed in Fig. 1b, and the Nomex attached to the facet is also shown in Fig. 1c with an area, where the BVID is made.

The following damage cases are in the paper:

1. BVID's of the diameter 1.4 and 1.8 cm.
2. Hole of 0.5 cm diameter.

The SLDV is an NDT device largely used in the industries for analyzing the vibrations of the structures. The SLDV instrument used is PSV 400 from Polytec© GmbH. The laser vibrometry uses the Doppler effect for non-contact optical vibration analysis. This uses light as a sensor and thus a contactless experimental process. This

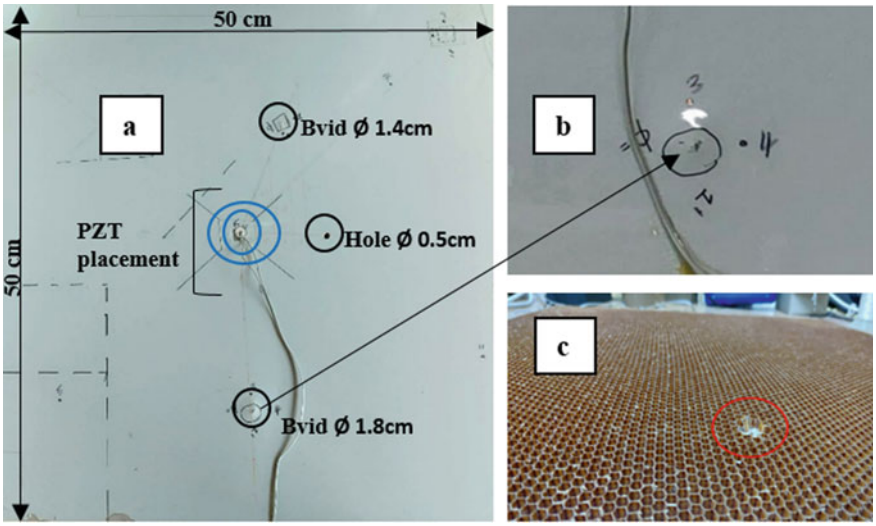

Fig. 1 **a** SCS plate with damages, **b** zoomed portion of BVID of $\emptyset = 1.8$ cm, and **c** Nomex core attached at the backside of the plate and region, where BVID is made

gives real-time measurements on temporal signatures. It works on the frequency of laser shift between the reference beam and the incident beam from the laser. The interferometer inside the laser head analyses this shift by propagating them to the photodetector. Thus, depending on the velocity, the backscattered light gets changed in frequency and phase.

Thus, the Doppler shift in frequency is analyzed based on the modulated detected output signals. Thus, after performing inbuilt signal processing techniques, the velocity and displacement of the structure surface are detected. The laboratory setup of LDV is shown in Fig. 2. The PZT's are bonded with bonding glue to the plate. A sine tone bursts signal with 10 cycles and with an amplification value of 16 V_{PP}, and gain of 20 (16 × 20) produces the excitation. The total number of grid points and frequency used in the experiment is summarized as follows in Table 1.

For the spectral element method (SEM), a hole of Ø 0.5 cm is studied. The engineering constants used for the analysis are highlighted in Table 2. The parameters used in SEM are explained in Tables 3, 4, and 5.

Dielectric, electromechanical, and mechanical properties used for PZT (Sonox P502) is shown in Tables 3 and 4, respectively, where d_{33}, $d_{31,}$ d_{15} are charge constants, $\frac{\varepsilon_{33}^{T}}{\varepsilon_0}$, $\frac{\varepsilon_{11}^{T}}{\varepsilon_0}$ relative permittivity values, $S_{11}{}^{E}$, $S_{33}{}^{E}$ are elastic compliance values, ρ represents density value, and η_{13} represents the Poisson ratio.

The SEM technique, similarly to FEM, divides modeled domain into finite elements, imposing the arbitrary boundary conditions and external forces in the particular nodes. Distribution of the nodes in the element is the main difference between both methods, while the nodes in SEM are non–uniformly distributed. They

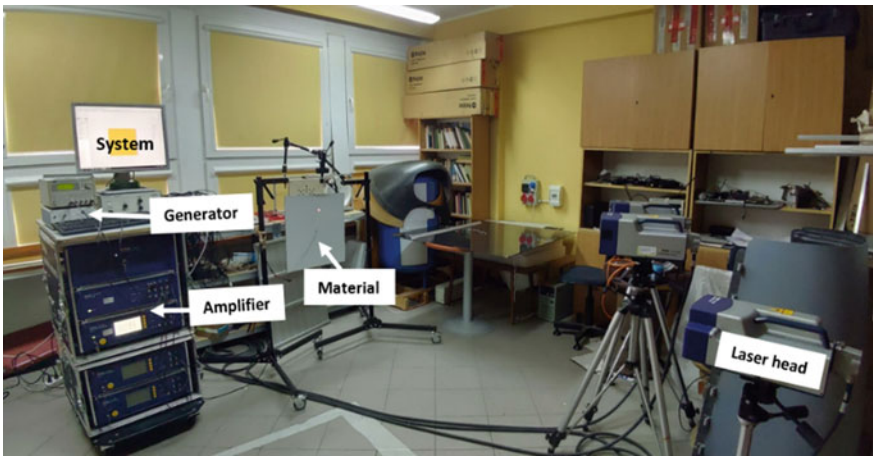

Fig. 2 LDV setup

Table 1 Experimental table with measurements performed in the LDV

No. of cycles	Frequency (kHz)	VPP	Grid points	Time increment (μs)
10	150	16	411 × 415	0.78125

Table 2 Engineering constants used in the numerical study

Material	Young's modulus (GPa)	Poisson ratio	Density (kg/m^3)
Nomex	9	0.30	1384
Aluminum	68	0.33	2600

Table 3 Electromechanical and dielectric properties of PZT

d_{33} (C/N)	d_{31} (C/N)	d_{15} (C/N)	$\frac{\varepsilon_{33}^T}{\varepsilon_0}$	$\frac{\varepsilon_{11}^T}{\varepsilon_0}$
440E−12	−185E−12	560E−12	1850	1950

Table 4 Mechanical properties of PZT and other values

$S_{11}{}^E$ (m^2/N)	$S_{33}{}^E$ (m^2/N)	η_{13}	ρ (kg/m^3)
18.5e−12	20.7e−12	0.44	7740

Table 5 Numerical table with values used

No. of cycles	Frequency (kHz)	Grid points	Time increment (μs)
10	150	251 × 251	6.1e−3

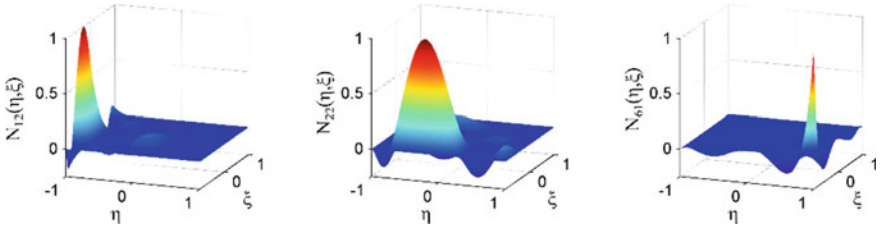

Fig. 3 Two-dimensional spectral shape function

are coincident with the coordinates of the Gauss–Lobatto–Legendre (GLL) integration points. Figure 3 and Eq. 1 depicts examples of 2D orthogonal shape functions which are constructed as a tensor product of $N_{\mathrm{m}}(\xi)$ and $N_{\mathrm{n}}(\eta)$.

$$N_{mn}(\hat{\imath}, \varsigma) = N_m(\hat{\imath})\, N_n(\varsigma), \text{ for } m = 1 \ldots\ p,\ n = 1 \ldots r \tag{1}$$

As a consequence of the orthogonality of shape functions as well as the application of GLL quadrature, the mass matrix is diagonal in the formulation. This property significantly reduces computation time for solving the equation of motion due to avoiding mass matrix inversion.

3 Results and Discussion

3.1 Analysis of the Results from the LDV

Velocity plots obtained directly from the LDV is analyzed. The lamb wave propagation of the specimen is visualized in Fig. 4. Figure 4a analyzed with 150 kHz frequency shows the propagation of the waves in the form of circles. The waves

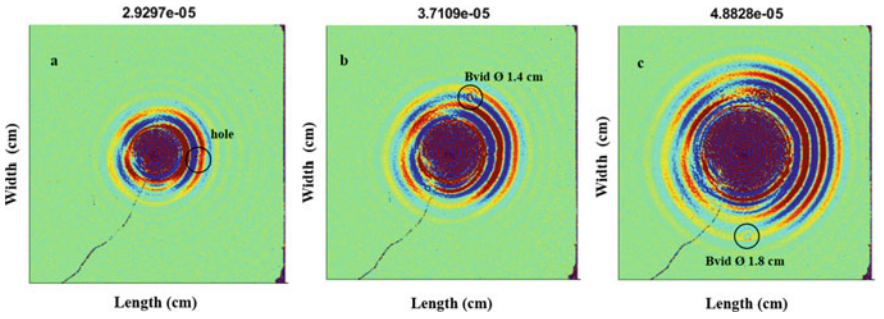

Fig. 4 **a** A hole of Ø 0.5 cm detected at 29 μs, **b** BVID of Ø 1.4 cm detected at 37 μs, and **c** BVID of Ø 1.8 cm detected at 48 μs

Table 6 Time where the damage gets detected

Frequency (kHz)	Hole (μs)	BVID1 (μs)	BVID2 (μs)
150	29	37	48

reach the damage region (hole) and get distracted, thus showing the location and damage shape. It shows the hole region perfectly with lamb waves getting scattered.

The experiment is carried out with a frequency range of 10, 15, 20, 25, 50, 100, 150, 200 kHz, and it is found that the 150 kHz frequency provides good visualization of results. The amplitude of the S0 mode is much lower than A0 mode; therefore, it is barely noticeable on the full field of the wave measured by the LDV. Thus, mostly, the antisymmetric A0 mode waves are clearly visible and marked in all the figures, respectively.

When the waves reach the damage zone, it gets reflected and mode change occurs. The important aspect is to visualize the wave reflections after it touches the impact damage zone. Thus, LDV helps in quality analysis of the material without destructing it. Figure 4b shows the BVID Ø 1.4 cm, getting detected. The waves get scattered at the damage region (marked with black circles), and mode change occurs. Figure 4c shows the wave pattern analysis and detection of BVID of Ø 1.8 cm.

The LDV measures the out of plane displacement and helps in the early inspection. As shown in Fig. 4, one can visualize the *S* waves reaching the damage region and its conversion. This shows a clear visualization of the damage. The time for the waves to reach the damage zones is summarized as follows in Table 6.

3.2 Analysis of the Results from Numerical Studies

In this section, the numerical results from the SEM are shown. Thus, the main idea is to check the experimental results visualized with the numerical studies and to put a proper comparison of the results. For this spectral elemental study, a hole Ø 0.5 cm section is selected to be analyzed. Figure 5a shows the mesh arrangement and PZT position in the SEM approach; Fig. 5b shows the result obtained with the SEM numerical study.

Thus, a comparative study of numerical analysis and experimental results has shown that the hole gets detected at a time period of 29 μs in both cases as shown in Figs. 4a and 5b, respectively. Thus, by comparing the experimental and numerical figures, 4 and 5 reveal the wave field of the lamb waves and its change due to the damage zones, respectively.

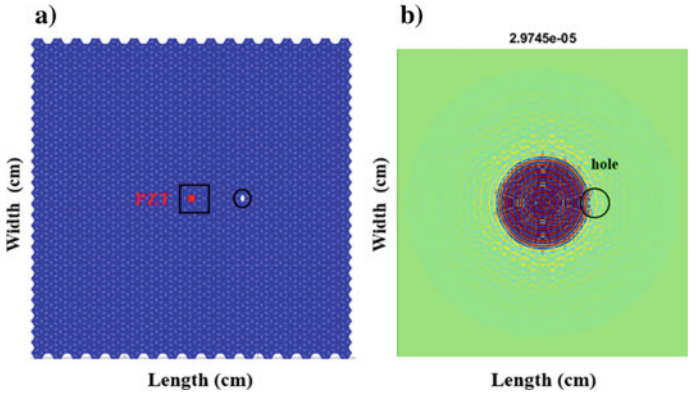

Fig. 5 **a** Mesh arrangement and PZT position in SEM, **b** hole of Ø 0.5 cm detected at 29 μs for 150 kHz excitation

3.3 Analysis of the Results Using an Elliptical-Based Signal Processing Method

The numerical data from SEM is used to locate the damaged region. This section focuses on the application of the elliptical-based signal processing method in localizing the damage [14]. The concept behind is the intersection of the ellipses and at the region where a large number of ellipses intersects, thereby identifying the region of damage with higher energy. Optimum sensor positioning and damage localization are considered. Three cases with different sensor positioning are shown in Table 7. Cases 1 and 3 are taken from research on the optimal sensor placement assisted with a genetic algorithm [15].

For the elliptical-based method to function, a velocity profile is to be determined because the velocity can be angle-dependent. Thus, the velocity of the waves is determined. The steps performed to obtain the velocity profile are summarized below and with Eq. 2.

The scanning points are placed at equal distances, and thus, the velocity of the waves is calculated based on the formulae shown below.

$$\text{Velocity} = \frac{\text{delx}}{\text{delt}} \tag{2}$$

Table 7 Case models for elliptical approach with experimental and numerical data

Case	Test	Sensor placement	Frequency (kHz)	PZT	No. of sensing points
1	Experimental	Quadrant I, II, III, IV	150	Center	8
2	Numerical	Quadrant II	150	Center	6
3	Numerical	Quadrant I, II, III, IV	150	Center	8

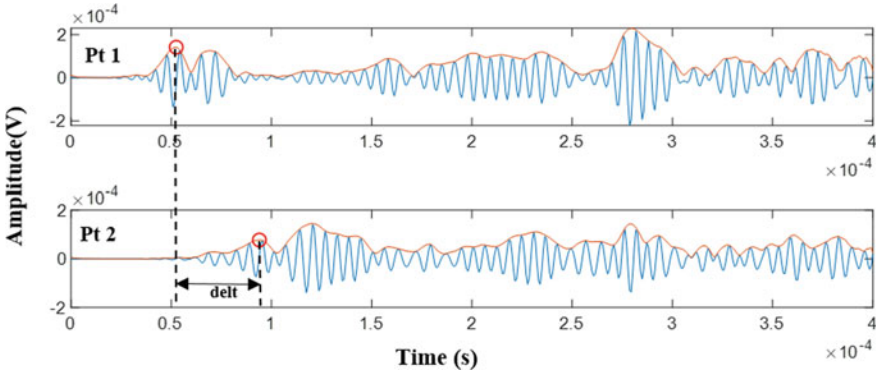

Fig. 6 Delt calculation between two points

where delx is the distance between the scanning points, and delt is the distance between the max peak value of the first wave packet of one point to the similar max peak value of another point. The calculation of delt between pt1 and pt2 of case 2 signals is shown in Fig. 6. The velocity profile is calculated by taking 0°, 90° scanning points of case 2. It is then used to calculate the entire 360° values and marked with a polar plot in Fig. 7 indicating an almost perfect isotropic profile. These velocity profile values obtained are used for case 1 and 3 calculations, respectively.

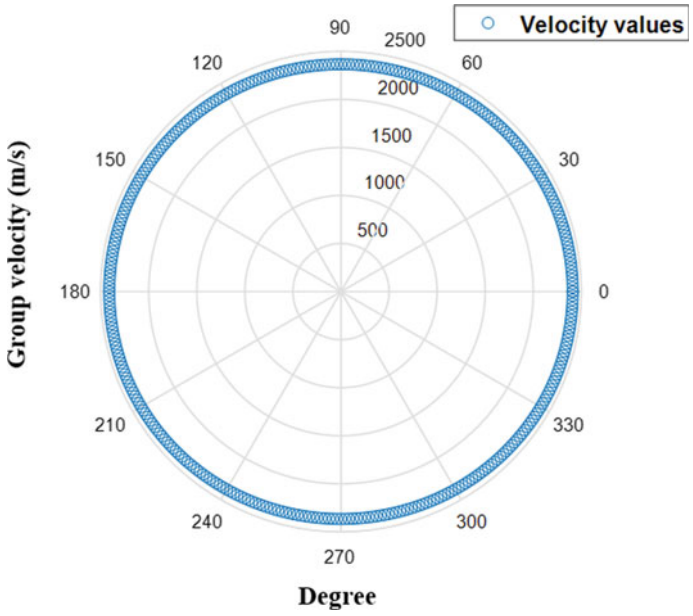

Fig. 7 Velocity profile obtained

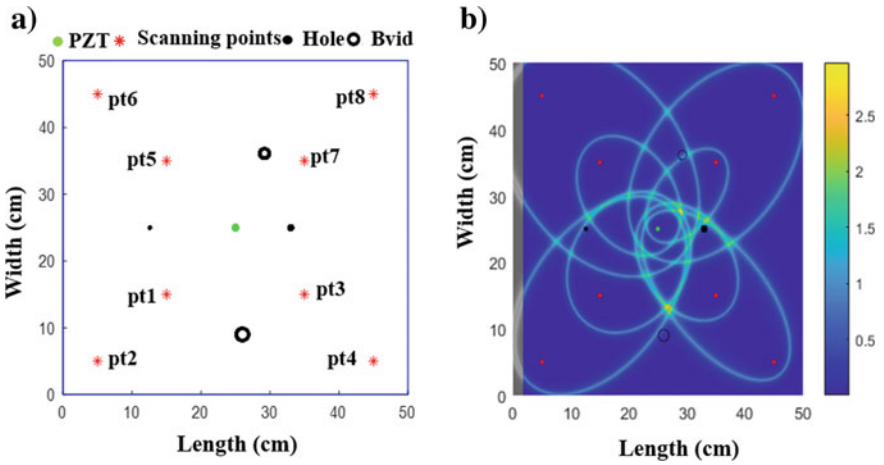

Fig. 8 Experimental case: **a** case 1 quadrant I–IV arrangement of sensors, **b** elliptical method on case 1

The elliptical method is applied to the complete experimental case 1 with 2 BVIDs and hole as shown in Fig. 8a. The results tried to identify most of the damage locations but in some cases, it could not due to multiple damage locations and thereby causing multiple reflections as shown in Fig. 8b. Thus, the research is later shifted to the data obtained from a numerical study which was simpler due to only one damage and gave good clarity of results as shown in Fig. 9.

Figure 9 shows the calculation performed and the damage located, respectively. Figure 9a, b shows the sensor network placements in two cases. The analysis of the results from Fig. 9 shows the region of higher energy, where ellipses get coincident more. In Fig. 9c, the damage hole region is properly detected with the help of intersecting ellipses. The higher energy is due to wave reflection from the damage. This result is obtained by analyzing results from various peak values extracted from the time signals.

In Fig. 9c, the scanning sensor points are placed at an interval of 10 cm and located at 0°, 45°, and 90°, respectively. The highest reflection is obtained at a distance of (31.9, 26) cm^2, whereas the damage is at (33, 25) cm^2. Thus, the high energy reflection from the damage is captured at a distance of 1.49 cm from the actual damage location.

In a similar way for Fig. 9b, the scanning points are placed at all quadrants of a square plate (according to [15]). This resulted in more convergence of ellipses and more scanning sensor points as shown in Fig. 9d. The highest convergence of ellipses reflection is obtained at a distance of 4.1 cm from the damage location. The damage location is at (33, 25) cm^2, and the maximum reflection is obtained at (29.8, 27.8) cm^2. Case 2 analysis gave more precise results when compared to case 3.

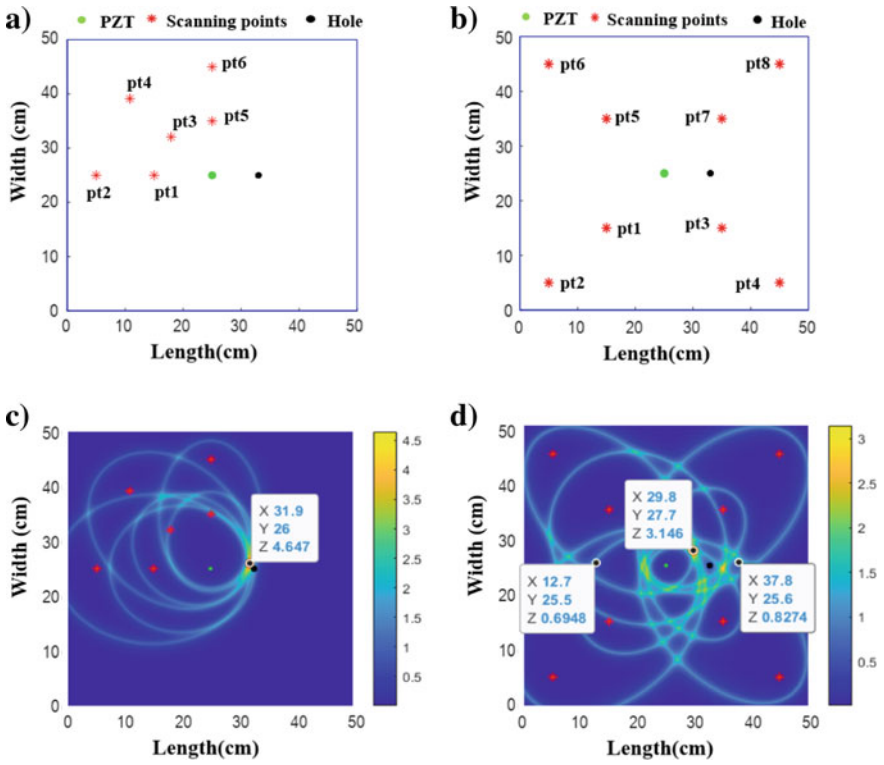

Fig. 9 Numerical cases: **a** case 2 quadrant II arrangement of sensors, **b** case 3 quadrant I–IV arrangement of sensors, **c** elliptical method on case 2, and **d** elliptical method on case 3

4 Conclusion

The research purposed is about the NDT inspection of barely visible impact damage (BVID) in the aluminum Nomex SCS plate using guided wave propagation. The damage regions are successfully analyzed with the help of the A0 wave mode. The lamb waves interactions and impact damages produced are visualized and are detected. The frequency of excitation at 150 kHz is chosen after studying different frequency ranges. The lower excitation frequencies (10, 15, and 50 kHz) were studied, and it failed to capture the damage results. Thus, further increase in the frequency like 100, 150, 175, and 200 kHz gave good quality results. The results from the LDV gave a good appropriate identification of the damage location. This gave a good analysis of wave pattern study and mode changes in the damage region. The lamb wave propagation and reflection from damages are identified with LDV and shown in Fig. 4. The LDV results identify the two different BVID damages and the small hole with the help of guided waves.

The spectral elemental code is used to analyze similar conditions numerically. The results obtained from it identified the damage at a similar time period as the experimental case. The elliptical signal processing technique works on the methodology of visualization of the wave reflection site. The interaction of the wave with damage creates higher energy reflected zone. In this method, three different cases are studied as shown in Table 7. Case 1 corresponds to the result obtained from experimental studies (LDV), and cases 2 and 3 are from SEM calculations. The sensor network positions are different for all three cases. Case 2 provided a better result in identifying the damage location. Thus, by using the elliptical-based signal processing technique, the data obtained from LDV and SEM is again used to locate the damaged region. Thus, overall a case study of experimental, numerical, and analytical studies is carried out to understand the wave propagation phenomenon and to locate the damage with sensor network arrangements.

Acknowledgments The authors would like to acknowledge the support funding provided by the National Science Center, Poland under SONATA BIS project titled: Study of piezoelectric sensors placement and their interaction with structural elements (2016/22/E/ST8/00068).

The research was also funded by the Polish National Science Center under grant agreement no UMO-2018/31/N/ST8/02865 in the frame of PRELUDIUM project entitled: Model-assisted damage identification function for Structural Health Monitoring of composite structures under a varied environmental condition.

The authors also acknowledge Task-CI for allowing the use of computational resources.

References

1. Guo N, Cawley P (1993) The interaction of Lamb waves with delaminations in composite laminates. J Acoust Soc Am 94:2240–2246
2. Toyama N, Yamamoto T, Urabe K, Tsuda H (2017) Ultrasonic inspection of adhesively bonded CFRP/aluminum joints using pulsed laser scanning. Adv Compos Mater
3. Diamanti K, Hodgkinson JM, Soutis C (2004) Detection of low-velocity impact damage in composite plates using Lamb waves. Struct Health Monit 3:33–41
4. Hayashi T, Kawashima K (2002) Multiple reflections of Lamb waves at a delamination. Ultrasonics 40:193–197
5. Park B, An YK, Sohn H (2014) Visualization of hidden delamination and debonding in composites through noncontact laser ultrasonic scanning. Compos Sci Technol 100:10–18
6. Sikdar S, Kudela P, Radzienski M, Kundu A (2018) Online detection of barely visible low-speed impact damage in 3D core sandwich composite structure. J Compos Struct 185:646–655
7. Philbert M, Soutis C, Gresil M, Yao K (2018) Damage detection in a composite T-joint using guided lamb waves. Aerospace MDPI 40:1–13
8. Ruzzene M, Joeng SM, Michaels TE, Michaels JE, Mi B Simulation and measurement of ultrasonic waves in elastic plates using laser vibrometry
9. Patera AT (1984) A spectral element method for fluid dynamics: laminar flow in a channel expansion. J Comput Phys 54:468–488
10. Kudela P, Zak A, Krawczuk M, Ostachowicz W (2007) Modelling of wave propagation in composite plates using the time domains spectral element method. J Sound Vib 302:728–745
11. Kudela P, Ostachowicz W (2009) 3D time-domain spectral elements for stress waves modelling. J Phys Conf IOP publishing 181:1–9

12. Ha S, Chang FK (2009) Optimizing a spectral element for modeling PZT-induced lamb wave propagation in thin plates. Smart Mater Struct 19:1–12
13. Ge L, Wang X, Wang F (2014) Accurate modeling of PZT induced lamb wave propagation in structures by using a novel spectral finite element method. Smart Mater Struct 23:1–15
14. Fendzi C, Mechbal N, Rebillat M, Guskov M, Coffignal G (2015) A general bayesian framework for ellipse-based and hyperbola-based damage localisation in anisotropic composite plates. J Intell Mater Syst Struct 1–32
15. Soman R, Malinowski P (2019) A real-valued genetic algorithm for optimization of sensor placement for guided waves based structural health monitoring. J Sens